Int J Appl Earth Obs Geoinformation 64 (2018) 96–103

Contents lists available at ScienceDirect

Int J Appl Earth Obs Geoinformation

journal homepage: www.elsevier.com/locate/jag

Land-atmosphere interaction patterns in southeastern South America using satellite products and climate models

P.C. Spennemann[a,*], M. Salvia[b], R.C. Ruscica[a], A.A. Sörensson[a], F. Grings[b], H. Karszenbaum[b]

[a] Centro de Investigaciones del Mar y la Atmósfera (CONICET/UBA), UMI-IFAECI (CONICET/CNRS/UBA), Buenos Aires, Argentina
[b] Instituto de Astronomía y Física del Espacio (IAFE–CONICET/UBA), Buenos Aires, Argentina

ARTICLE INFO

Keywords:
Land-atmosphere interaction
Southeastern South America
Satellite products
Soil moisture
Land surface temperature
Climate modelling

ABSTRACT

In regions of strong Land-Atmosphere (L-A) interaction, soil moisture (SM) conditions can impact the atmosphere through modulating the land surface fluxes. The importance of the identification of L-A interaction regions lies in the potential improvement of the weather/seasonal forecast and the better understanding of the physical mechanisms involved. This study aims to compare the terrestrial segment of the L-A interaction from satellite products and climate models, motivated by previous modeling studies pointing out southeastern South America (SESA) as a L-A hotspot during austral summer. In addition, the L-A interaction under dry or wet anomalous conditions over SESA is analyzed. To identify L-A hotspots the AMSRE-LPRM SM and MODIS land surface temperature products; coupled climate models and uncoupled land surface models were used. SESA highlights as a strong L-A interaction hotspot when employing different metrics, temporal scales and independent datasets, showing consistency between models and satellite estimations. Both AMSRE-LPRM bands (X and C) are consistent showing a strong L-A interaction hotspot over the Pampas ecoregion. Intensification and a larger spatial extent of the L-A interaction for dry summers was observed in both satellite products and models compared to wet summers. These results, which were derived from measured physical variables, are encouraging and promising for future studies analyzing L-A interactions.

L-A interaction analysis is proposed here as a meeting point between remote sensing and climate modelling communities of Argentina, within a region with the highest agricultural and livestock production of the continent, but with an important lack of in-situ SM observations.

1. Introduction

The identification of regions where the land surface condition has a significant impact on the atmosphere is crucial to improve our understanding of regional and local climate. In these regions −called hotspots-, soil moisture (SM) variability has the potential to modulate the atmospheric conditions through changes in the latent- and sensible-energy fluxes on time scales ranging from diurnal to seasonal (Seneviratne et al., 2010). SM influence on precipitation is predominant during the summer season, when energy fluxes are high enough to trigger convection. As SM anomalies persist longer than atmospheric ones, L-A interactions can also contribute to the intensification and persistence of extreme temperature events (Mo and Berbery, 2011); for example low soil moisture values reduce the evaporative cooling, increasing the atmospheric heating through sensible heat fluxes (Hirschi et al., 2014; Seneviratne et al., 2010). Therefore, an improved knowledge of L-A interactions and more realistic SM data for atmospheric models can improve weather and seasonal forecast skills over these hotspot regions. In transition zones between dry and wet climates, SM is in general characterized by medium range values and high variability, giving the potential conditions for strong L-A interactions (Koster et al., 2004).

Conceptually, L-A interaction can be divided in two segments; the terrestrial and the atmospheric. The terrestrial segment involves the direct influence of SM anomalies over surface variables such as temperature or evapotranspiration through their influences on the partitioning of latent and sensible heat fluxes (Dirmeyer, 2011). This mechanism has been confirmed over regions with water-limited regimes where the partitioning of available energy is sensitive to changes in SM conditions (Fig. 2a of Entekhabi et al., 2010). The atmospheric segment, i.e. SM influence (through evapotranspiration or temperature) on precipitation, is of high complexity since it involves thermodynamic and dynamic atmospheric processes on a wide range of temporal and spatial scales (e.g. Ruscica et al., 2015). Here, the “interaction” and “coupling” terms follow the definitions given in Seneviratne et al. (2010).

Land surface models (LSMs) represent processes ranging from basic

* Corresponding author.
E-mail address: p.spennemann@gmail.com (P.C. Spennemann).

http://dx.doi.org/10.1016/j.jag.2017.08.016
Received 7 February 2017; Received in revised form 14 August 2017; Accepted 31 August 2017
Available online 14 September 2017
0303-2434/

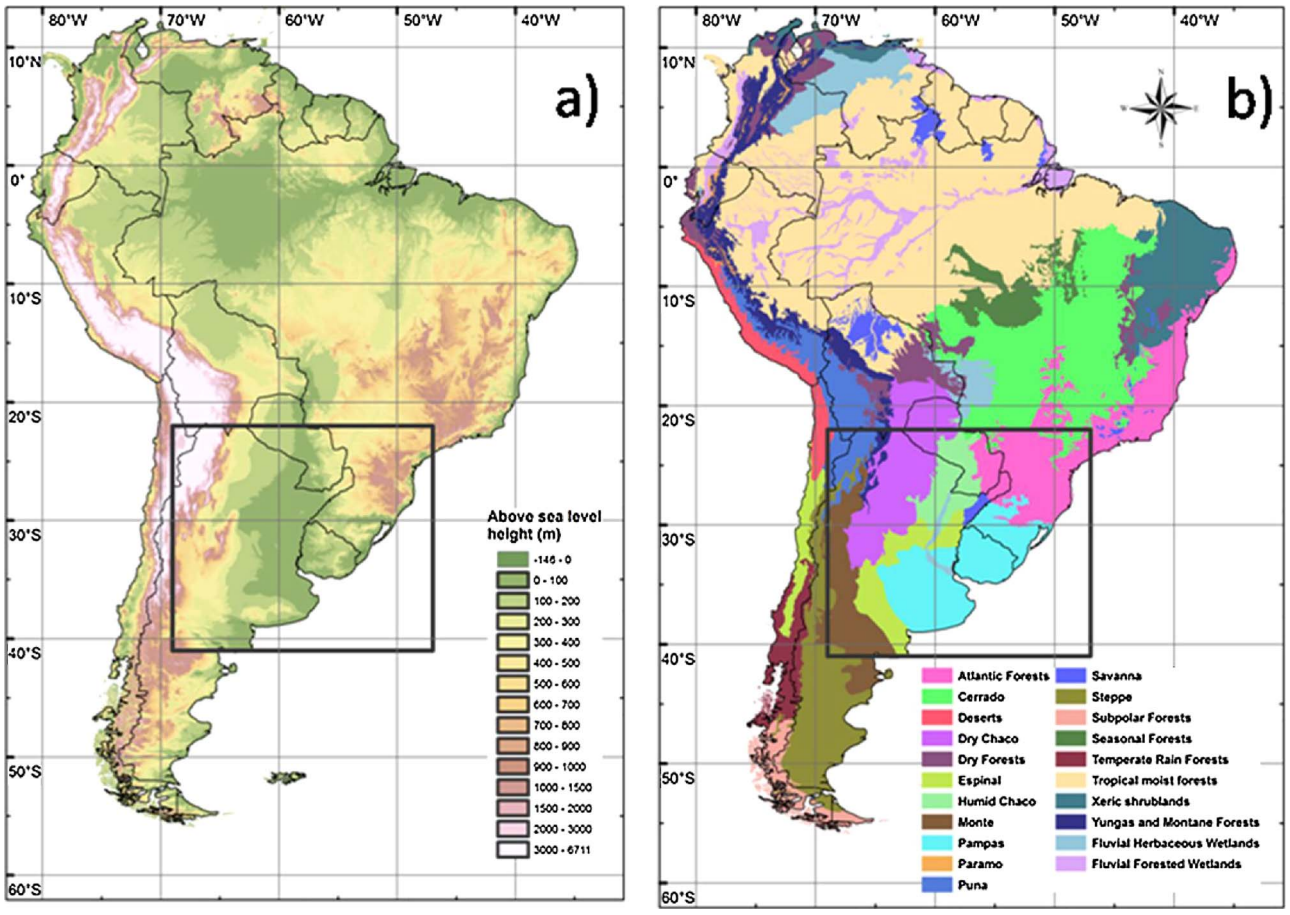

Fig. 1. a) Topography and b) Ecoregions over South America. Black box denotes SESA region. Topography data: 30 s conditioned DEM from HydroSHEDS (Lehner et al., 2006). Ecoregions have been modified from Terrestrial Ecosystems of the World (TEOW, Olson et al., 2001).

water and energy balances to complex biogeochemical interactions and dynamic vegetation (Sato et al., 2015). The atmospheric input to the LSM usually comes from an atmospheric model (coupled mode) or observations (uncoupled mode). Surface SM is among the most complex hydrologic variables to simulate as it interacts with the atmosphere, plant canopy and roots, and vadose zone (Du et al., 2016). In this sense, the main limitations of LSMs are related to uncertainties in the representation of the land surface information like vegetation (e.g. greenness fraction, leaf area index, stomatal resistance), land cover (e.g. surface roughness, albedo, emissivity) and soil-types (texture).

Climate and weather/seasonal forecasts are performed by numerical models that consist of physical equations that describe the components of the climate system and their interactions (Stensrud, 2007). In particular, in these numerical models the atmosphere is coupled to a LSM.

Global studies show that for summer, southeastern South America (SESA) is characterized as a water-limited region (Jung et al., 2010) and identified as a L-A interaction hotspot (e.g. Wang et al., 2007; Zeng et al., 2010). Hirschi et al. (2014) and Mueller and Seneviratne (2012) found a negative correlation between SM conditions and the number of hot days of the warmest month, thus highlighting the strong L-A interaction over the region of SESA.

Several continental-scale studies also found L-A hotspots over SESA, using different variables, models and statistical approaches. Among them, Sörensson and Menéndez (2011) found that the main summer hotspot of both evapotranspiration and precipitation is located within SESA using ad-hoc experiments to isolate the influence of SM on atmospheric variables. The same methodology was used in Ruscica et al. (2015), showing that coupling is stronger during anomalously dry summers. Studies using various statistical approaches applied to different datasets found strong L-A interaction in the same region (e.g. Spennemann and Saulo, 2015; Ruscica et al., 2016).

The scarcity of in-situ SM observation networks hinders a validation at regional scales, particularly in South America (https://ismn.geo.tuwien.ac.at/networks/). Alternatively, the recent availability of land surface variables −like SM- derived from multiple remote sensing products, allows the evaluation of L-A interaction based on simulations at global scale (Ferguson et al., 2012; Hirschi et al., 2014; Gallego-Elvira et al., 2016). The instruments operating in the microwave portion of the spectrum have received attention because this frequency range has the unique ability to return information on media (atmosphere, vegetation, soil) that are opaque to shorter visible/near-infrared and thermal wavelength and because microwave scattering and emission are directly related to the water content of the target. In particular, remote sensing from active and passive microwave sensors have demonstrated to be good and flexible tools for observing the SM content of the first centimeters of soil and for detecting its spatial and temporal variations from radar (e.g. Barret et al., 2009; Notarnicola et al., 2006) and radiometric microwave sensors (e.g. Jackson, 1993; Mladenova et al., 2014).

Satellite-derived SM products have benefited from ongoing improvements in the instrument and retrieval algorithm. Currently, several global SM products have become available (Sakai et al., 2016). The availability of in-situ SM observations to validate the products has also significantly increased, but mainly in the northern hemisphere (Dorigo et al., 2011).

Motivated by evidences of climate models that point out SESA as a L-A hotspot and by the availability of consistent time series of satellite products, this study aims at answering the following questions: 1) Do satellite estimations reproduce the terrestrial segment of the modelled summer L-A interaction over SESA? 2) Is this interaction enhanced or

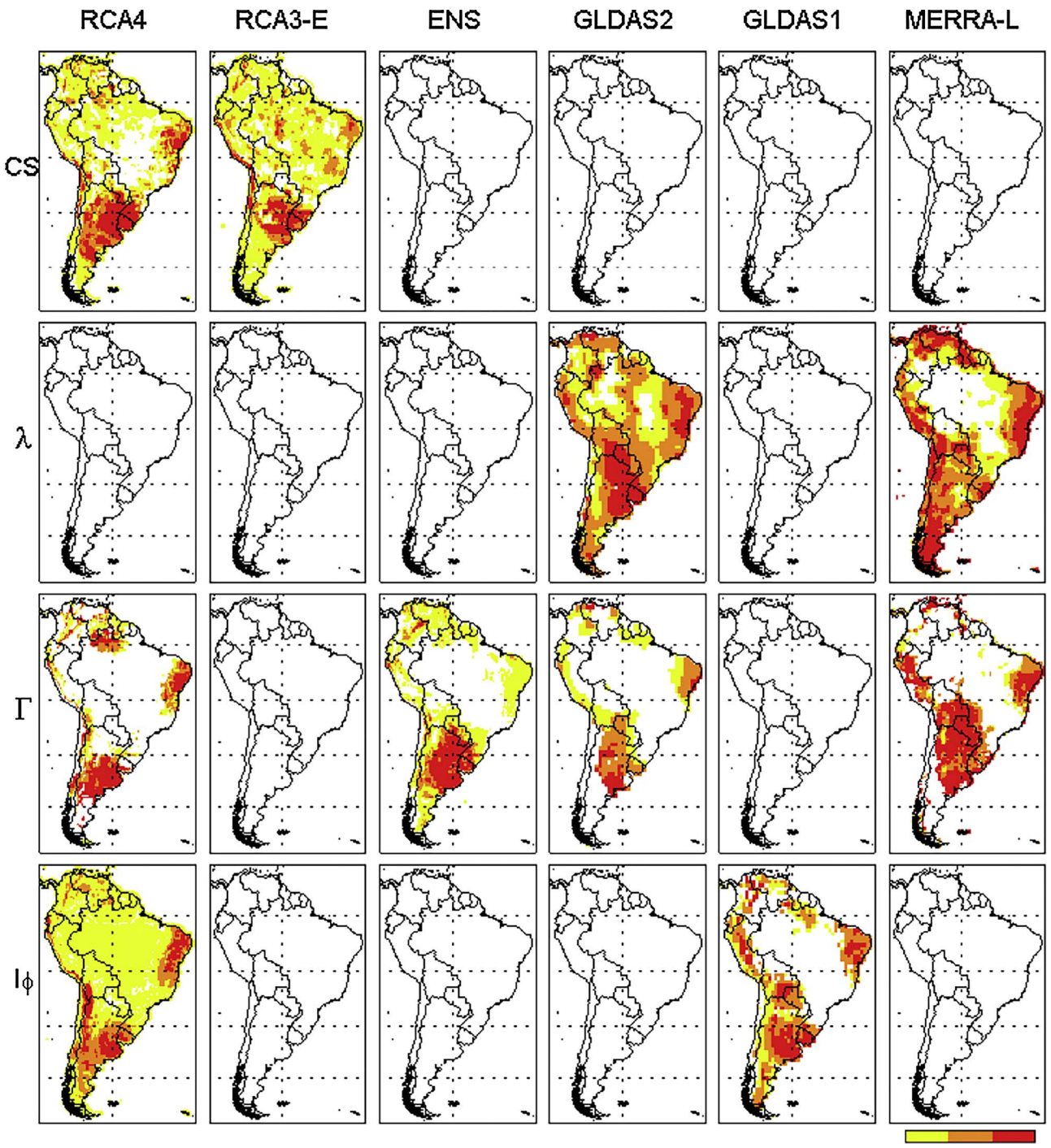

Fig. 2. Modeled terrestrial-segment of L-A interaction in South America for summer (DJF). Models and L-A interaction indices are shown in columns and rows respectively. Grid points with strong, medium and low L-A interaction are shown in red, orange and yellow respectively. Intensity values are not displayed due to differences in metrics, periods, temporal scales and variables used. (For interpretation of the references to colour in this figure legend, the reader is referred to the web version of this article.)

diminished under dry or wet anomalous conditions over the region?

The region of study, the models and satellite products, and the L-A index employed are described in Section 2. Results and discussion are presented in Section 3, where several model (coupled and uncoupled) experiments and L-A interaction metrics over the region are presented, in order to analyse the satellite estimations. Then, the physical consistency of the satellite and model L-A interaction patterns are compared for anomalous wet and dry seasonal events. Finally, Section 4 presents authors conclusions.

2. Data and methods

2.1. Study region and its climatic characteristics

The diverse precipitation and temperature regimes together with the complex topography of the South American continent (Fig. 1a) create the conditions for the development of a vast variety of ecoregions (Fig. 1b), ranging from desert to forest and from dry regions to wetlands. However, many of these natural ecosystems have been modified through human activities (i.e. agricultureand cattle raising).

SESA (Fig. 1) expands between 40.5°-22.5°S and 67.5°–47.5°W.

SESA includes the southern part of La Plata Basin, the second largest basin of South America, with over 70 million people and 80% of the Gross Net Production of the 5 countries sharing the basin (Argentina, Brazil, Bolivia, Paraguay and Uruguay).

2.2. Observations: remote sensing products

2.2.1. Soil moisture and vegetation optical depth products

When selecting a satellite SM product for climatic applications, quality and length of the time series are of great importance. Although merged products exist, such as the ESA CCI SM product (http://www.esa-soilmoisture-cci.org/), the different instruments, temporal windows and spatial scales involved make these products not straightforward to use.

Our approach is to prioritize the SM product being directly related to the physical variable (i.e. microwave brightness temperature) measured by a specific instrument, and selecting among the individual products the one with the longest temporal series in order to obtain the largest amount of data. Thus, the SM product retrieved from the Advanced Microwave Scanning Radiometer-Earth Observing System (AMSRE-EOS) was selected, using the Land Parameter Retrieval Model (LPRM, Mo et al., 1982; Meesters et al., 2005).

The LPRM is based on a forward radiative transfer model to retrieve surface SM and Vegetation Optical Depth (VOD) from microwave brightness temperatures. The AMSRE-LPRM product is available in two files per day, one ascending (daytime) and one descending (night-time), archived as two different products. Here the night-time product was used, since studies (Njoku et al., 2003; Norouzi et al., 2011) show that it has a better performance, related with more uniform temperature and moisture profiles during the night time overpass. The AMSRE-LPRM product covers from June 2002 to October 2011 (when the AMSRE stopped producing data). SM and VOD products are analyzed over South America on a spatial resolution of 0.25° and on a temporal resolution of 8-day mean values to be comparable with Land Surface Temperature (LST) data (Section 2.2.2).

2.2.2. Land surface temperature product

The surface temperature was used, since the partitioning of surface fluxes in climate regimes with L-A interaction has a direct influence on this variable. Furthermore, satellite temperature products are more reliable than evapotranspiration products, since the thermal emission measured by satellites is directly related to the LST, while for the estimation of terrestrial evapotranspiration several measured variables and a mathematical model to combine them are needed (McCabe et al., 2013; Martens et al., 2016).

In this study the daytime LST from MODIS level-3 product MOD11A2 was used. This product is composed from the daily 1-kilometer LST product (MOD11A1) and from the average value of clear-sky LSTs during an 8-day window. The LST and Emissivity daily data are retrieved at 1 km pixels by the generalized split-window algorithm (Wan and Dozier, 1996).

The product's Quality Band (Wan, 1999, 2006) was used to filter out pixels with bad quality data. The area of South America was extracted and re-gridded from 1 Km filtered data to 0.25° regular grid. MODIS LST accuracy is of 1 K at 1 km resolution under clear sky conditions (Wan, 1999) and has a precision of 0.75 K in the temperature range of −35 °C to 75 °C (Zhou et al., 2014).

2.3. Models

Previous studies addressed different aspects of L-A interaction over the continent (Sörensson, 2010; Sörensson and Menéndez, 2011; Ruscica 2015; Ruscica et al., 2014, 2015, 2016; Spenneman and Saulo, 2015). They used several regional climate models (RCMs) as well as uncoupled LSMs. Some of their results are summarized in Fig. 2, showing in general strong L-A interaction over SESA. Two of these models were used in the present study: RCA4 (Samuelsson et al., 2011), and GLDAS-1 (Rodell et al., 2004) with the Noah LSM (version 2.7, Ek et al., 2003).

The top SM layer from RCA4 (7 cm) and Noah (0–10 cm) were used. The SM and temperature derived from models were averaged over 8-days in order to be comparable with the LST composites.

2.4. L-A interaction metrics

L-A interaction can be represented by statistical metrics/indices, quantifying the contribution that land surface has on the atmosphere. In Fig. 2 four different indices have been used. The CS index (Koster et al., 2004) quantifies the coupling between SM and any other atmospheric variable, and it requires controlled model experiments. The L-A interaction indices λ (Notaro, 2008) and Γ (Zeng et al., 2010) quantify the control of SM on precipitation and on evapotranspiration respectively using long data series of monthly mean values from any source (models, observations). The I_{Φ} index (Dirmeyer, 2011) can be used for data series with a temporal resolution down to 1-day and it quantifies the terrestrial segment of the L-A interaction.

The variables and temporal scale of the datasets used in this study determine that I_{Temp} index is the most appropriate, mainly because of the possibility of applying it on relatively short periods of time (9 years restricted by AMSRE availability) and high temporal resolution (8-day means restricted by MODIS). The I_{Temp} index (where Temp highlights that it quantifies the interaction between SM and temperature) is defined as

$$I_{Temp} = -\beta_{SM-Temp} * STD_{SM} \quad (1)$$

where the STD_{SM} is the total SM standard deviation, and $\beta_{SM\text{-}Temp}$ the slope of the linear regression between SM and LST anomalies (i.e. removing the mean value for each corresponding date). I_{Temp} is calculated over a total of 117 time values (13–eightday-means- per DJF x 9 DJFs (2003–2011)) and for every grid point. This index quantifies the sensitivity of surface variables to SM temporal variability. The product of β and STD takes into account both the correlation between SM and temperature and the potential for SM variations to result in large temperature fluctuations. To retain only grid points with a robust SM-LST relationship the following criteria were applied: 1) for each grid point and time step, SM associated to values greater than 0.5 or with VOD ≥0.8 were removed in order to mask out unreliable SM values; 2) the calculation of $\beta_{SM\text{-}Temp}$ was performed only for grid points where the sample size was equal or greater than 30; and finally 3) only grid points with significant correlations (99% confidence interval, two tail *t*-Test) between SM and LST anomalies were considered.

3. Results and discussion

3.1. L-A interaction in models

The summer terrestrial-segment of L-A interaction over South America is shown in Fig. 2. RCMs include two versions of the RCA model and a multi-model ensemble from the CLARIS-LPB project (ENS, Boulanger et al., 2011). LSMs include two versions of Noah (version 2.7 and 3.3) corresponding to GLDAS-1 and 2.0 respectively and the MERRA-Land reanalysis (Reichle et al., 2011). Some of these results are already published as RCA4-CS in Ruscica et al. (2015); RCA3E-CS in Sörensson and Menéndez (2011); GLDAS 2.0-λ in Spennemann and Saulo (2015) and ENS-Γ Zeng in Ruscica et al. (2016). Novel combinations between models and indices are MERRAL-λ, RCA4-Γ, GLDAS-2.0-Γ, MERRAL-Γ and RCA4-I_{Φ}.

Despite using different methodologies the region of SESA highlights in all cases but one (MERRAL-λ combination). Thus, SESA shows to be a robust model-based hotspot of L-A interaction during summer. Next, L-A interaction spatial patterns based on satellite products are explored to

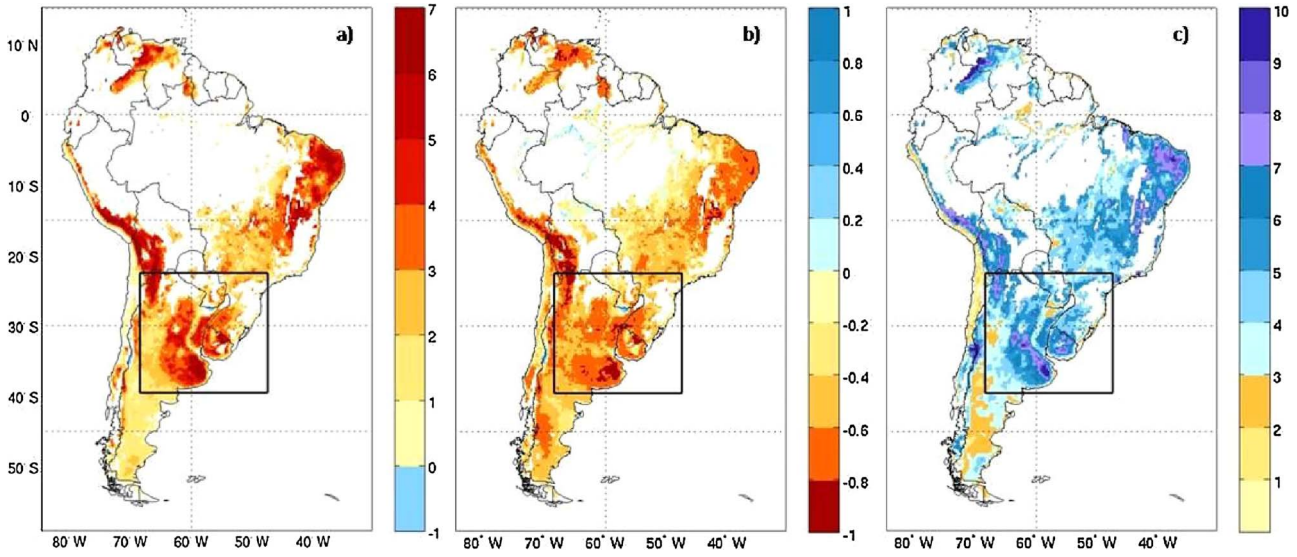

Fig. 3. a) Interaction Index (I_{Temp}) calculated for AMSRE-LPRM SM (X-band) and LST MODIS; b) Slope of the linear correlation between SM and LST anomalies (99% confidence interval, two tail t-Test); c) Temporal variability of SM, measured through Standard Deviation (STD) of absolute values series.

answer the question 1) mentioned in introduction.

3.2. L-A interaction in satellite products

The I_{Temp} index, described in Section 2.4, is calculated using the SM products from AMSRE-LPRM and LST from MODIS for summers of 2003–2011 (Fig. 3a). The strongest hotspots are localized in three large areas of the continent: the xeric shrubland region in Northeastern Brazil (NeB), SESA and Puna (Fig. 1b). Thus, the satellite L-A interaction shows an agreement over SESA and NeB with the results in Fig. 2. Puna hotspot lies on high and complex topography where data can present considerable uncertainties for SM retrieval (Ferguson et al., 2012; Abelen et al., 2015) as well as for models (e.g. Stensrud, 2007). Other smaller and lower intensity hotspots can be seen in central Brazil (Cerrado region), southern Chile (Valdivian Rainforest) and northwestern corner of the continent (Fluvial herbaceous wetlands). Fig. 3b and c display the two components of I_{Temp}; slope and variability (Eq. (1)). The sign of the resulting index is provided only by the slope, while the intensity of the interaction is related both to the slope and to the variability of SM.

Both SESA and NeB show high variability (STD SM $>$ 5), and steep slopes ($\beta < -0.6$). However, NeB shows larger areas with extremely high variability (STD SM $>$ 7), possibly related to the marked precipitation interannual variability (Zhou and Lau, 2001), while SESA shows larger areas with extremely steep slope ($-0.8 > \beta > -1$) indicating high sensitivity of temperature anomalies to SM anomalies. Although NeB is a robust hotspot, it will be not analyzed in this paper.

One important thing to remark is that the satellite I_{Temp} involves top soil layer SM and LST, which is not the case for the L-A interactions derived from models (Fig. 2) where some results used top- and other used whole column SM and 2-m temperature or surface fluxes is used instead of LST. On one hand, in a model, the SM of the whole column (2–8 m depending on model and region) influences on the 2-m temperature and surface fluxes, while there is no such physical coherence between AMSRE-LPRM SM and MODIS LST. On the other hand, in the coupled models, 2-m temperature and surface fluxes are determined by the interaction between the low atmospheric conditions and the SM, so they also depend on parameterizations of the atmospheric boundary layer, convection, etc. Furthermore, SM in coupled models is mainly driven by simulated precipitation that has its own biases. In the case of uncoupled models, SM is driven by observed near-surface atmospheric variables such as precipitation, radiation and winds. In this case, the 2-m temperature and surface fluxes depend strongly on these forcing data. Considering all these differences and the independency between satellite and model derived L-A interaction estimations, the hotspot location agreement is an encouraging result.

To examine the sensitivity of L-A interaction to the AMSRE band (C or X) used for the derivation of SM, Fig. 4a and b show the I_{Temp} index for both bands, and Fig. 4c shows the difference between them over SESA. Given the fact that SM is masked to avoid unreliable retrievals

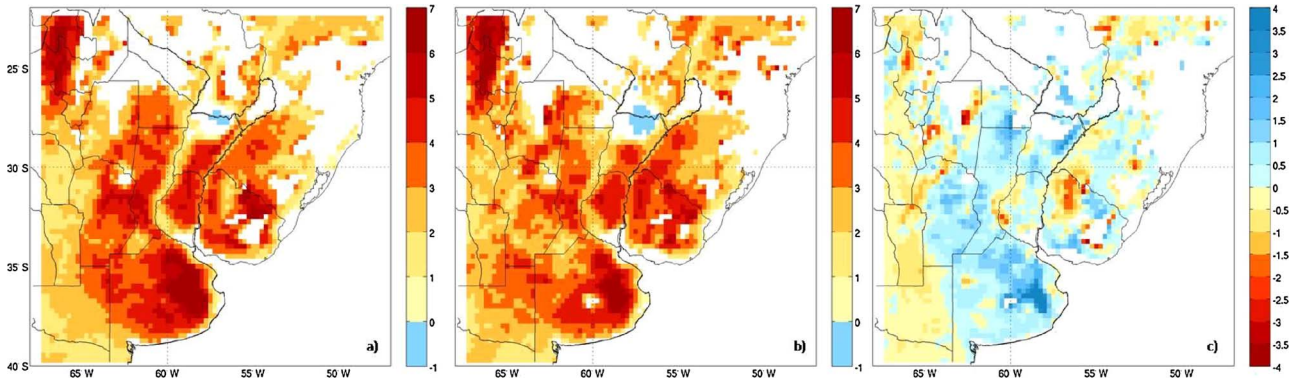

Fig. 4. a) L-A interaction Index (I_{Temp}) calculated for AMSRE-LPRM SM (X-band) and LST MODIS; (99% confidence interval, two tail t-Test); b) as in a) but for C band; c) Absolute difference between SM band X-band C. Red (blue) grid points show areas where L-A interaction is higher (lower) for C-band SM than for X-band. (For interpretation of the references to colour in this figure legend, the reader is referred to the web version of this article.)

due to dense vegetation, it is interesting to notice that for both bands similar areas are masked out. This is not trivial, since VOD depends not only of the vegetation biomass, but also on the relation between the sizes of the vegetation elements and the wavelength of the emitted microwave.

For both bands, I_{Temp} has its maximum values in the central-southern part of SESA (e.g. Pampa Húmeda, Uruguay and a small part of southern Brazil). The maximum located in the northwestern corner of the domain should be taken with caution because of its complex topography (Fig. 1a). Except for some isolated grid points surrounded by masked areas, there is only one large region with negative values which coincides with an unmasked permanent water body (Yaciretá dam) and the large wetland Esteros de Iberá, probably influencing the results.

The difference in the I_{Temp} index between C and X-band (Fig. 4c) shows a strong resemblance with the ecoregions in Fig. 1b. The I_{Temp} of X-band shows maximum values over Espinal, Pampas and Chaco Húmedo. These regions are characterized by: lower VOD compared to Chaco Seco (Espinal), seasonally variant VOD following the crop cycle (Pampas) or comprise wetlands or regularly flooded areas (blue in Fig. 4c). On the other hand, I_{Temp} of C-band shows higher values over the dryer ecoregions of Chaco Seco and Monte.

The differences between the SM(X) and SM(C) dynamical range address the sensitivity of I_{Temp} which is related to the type of ecoregion. In turn, the ecoregion defines the range of biomass density and wetness, both key parameters for the performance of the retrieval algorithm of the SM product used in this analysis.

As mentioned previously, model simulations show more sensitivity of surface fluxes to SM when anomalously dry conditions prevail. To analyze if L-A interaction based on satellite products, shares this characteristic, I_{Temp} is applied separately to anomalously dry and wet summers. The relative (%) mean seasonal SM anomalies were calculated to define wet and dry summers for the two AMSRE-LPRM bands and for the LSM Noah GLDAS-1 and the RCM RCA4. Two summers with dry and two summers with wet anomalies over the hotspot region of SESA were selected from the 2003–10 period (Fig. 5a, 2011 was excluded due to the simulated RCA4 period). Second, the precipitation mean seasonal anomalies were also calculated (Fig. 5b), as a way to evaluate the consistency of SM derived dry and wet summers. Finally, I_{Temp} was applied to the 2-summer temporal series of SM and LST (T2m for RCA4) for each database (Fig. 5c).

In general, satellite and modeled SM anomaly spatial patterns coincide between them and with precipitation anomaly patterns (Fig. 5a–b). The extreme drought of 2008-9 summer is observed with AMSRE and GLDAS-1, but is less evident in RCA4. This could be due to overestimated precipitation by RCA. On the other hand, all datasets show a marked positive (wet) anomaly during the summer of 2009–10. The largest difference between the two AMSRE-LPRM products is observed on the dry summer of 2005-06, where precipitation showed a larger resemblance with X-band than with C-band.

The satellite and modeled I_{Temp} spatial patterns for wet and dry summers are displayed in Fig. 5c. The dry I_{Temp} spatial patterns show considerable more grid points and higher values compared to the wet events, which is more evident for the satellite products, and in general the satellite I_{Temp} shows higher intensity compared to modeled I_{Temp}.

The AMSRE I_{Temp} hotspot for the dry summers strongly resembles the 2008–09 SM anomaly pattern, which is also evident for the dry anomalies on the western part of the domain for the wet 2002–03 event, while regions with wet anomalies show no significant L-A interactions. On the contrary, RCA shows L-A hotspots also for wet SM anomalies, although with lower intensity compared to the dry anomalies. The GLDAS-1 I_{Temp} hotspot is not so strongly related with the dry and wet SM anomalies, especially the hotspot of dry summers does not resemble the spatial extension of the very dry 2008–09 summer. Nevertheless, the location of the maximum values of I_{Temp} from GLDAS-1 and AMSRE show some similarities. The I_{Temp} differences might be related to the different depths of the top SM used by the models, the sensitivity of AMSRE X and C-bands to vegetation, the 2 m temperature used in RCA4 instead of the LST, and potential model parameterizations uncertainties representing the L-A interactions.

Fig. 5d shows a specific designed numerical experiment with RCA (Ruscica et al., 2015), focusing on the L-A interaction sensitivity between dry and wet summers, which motivated the previous analysis. The satellite and model I_{Temp} sensitivity to dry and wet events are in line with the strong L-A interaction sensitivity found by the author's, but a direct comparison between extension and intensity of the hotspot is not possible since another dry summer was used (1988–89) and a different methodology was applied.

Based on our analysis, both land surface models and satellite products identify similar patterns of relative mean seasonal anomalies of top SM and, dry soil conditions establish a stronger sensitivity of LST to SM in satellite products and in model simulations compared to wet conditions.

An interesting result observed in this study is that satellite L-A interactions are stronger compared to the modeled ones (GLDAS-1 and RCA4). This particular behavior is opposite to the results obtained by Hirschi et al. (2014). They observed a lower intensity in the satellite L-A interactions using monthly lagged correlations between satellite SM and the hottest month, compared with a SM proxy (i.e. Standardized Precipitation Index, SPI) and GLDAS-1 surface and root zone SM simulations. Although Hirschi et al. (2014) caution about the fact that the L-A interaction metric used could be influenced by the different sensors used over the period of study (1979–2010); from our perspective the opposite results (i.e. satellite stronger/weaker L-A interaction compared to models) are related with the different time scales used in both studies (SM 8-days mean vs. monthly means) and the L-A interaction metrics (simultaneous vs. monthly lagged). Since surface SM shows a more rapid response to precipitation and temperature (e.g. hours, days) than root-zone SM, we consider that using satellite surface SM products for L-A interaction estimations based on ~weekly and simultaneous basis are more suitable than on monthly and lagged estimations.

4. Conclusions

This study addresses two main subjects related to the assessment of summer L-A interaction based on satellite products. The first one is how well the combined use of AMSRE SM and MODIS LST products represents the L-A interaction spatial patterns over SESA, as defined by the L-A interaction metric considered in this work, and the second one is its behavior under dry and wet conditions.

First, a spatial pattern comparison of the L-A interaction derived from SM and LST satellite products against coupled and uncoupled models using different metrics was performed. The different metrics, temporal scales and independent datasets (i.e. models and satellite products) highlight the region of SESA as a strong L-A interaction hotspot, showing consistency in L-A interaction among satellite products and models.

As the L-A interaction calculation of this study uses the AMSRE-LPRM SM product, a band sensitivity analysis was performed over SESA. Both C and X-band were used to calculate the terrestrial segment of the L-A interaction, showing an agreement in the L-A hotspot location. However, the intensity values showed to be sensitive to the band, an issue which is presumably related to the different eco-region characteristics present in this area.

When dry and wet summers were compared, a larger spatial extent and an intensification of the L-A interaction for dry events were observed when the satellite products were used. This behavior was also observed in the model-based L-A interaction mainly over the Pampas ecoregion (central part of SESA), showing a physical consistency between model and the satellite derived L-A interaction. The possibility of following L-A interaction patterns based on the use of satellite products derived from measured physical variables, such as brightness temperatures in the microwave and thermal infrared region, is encouraging

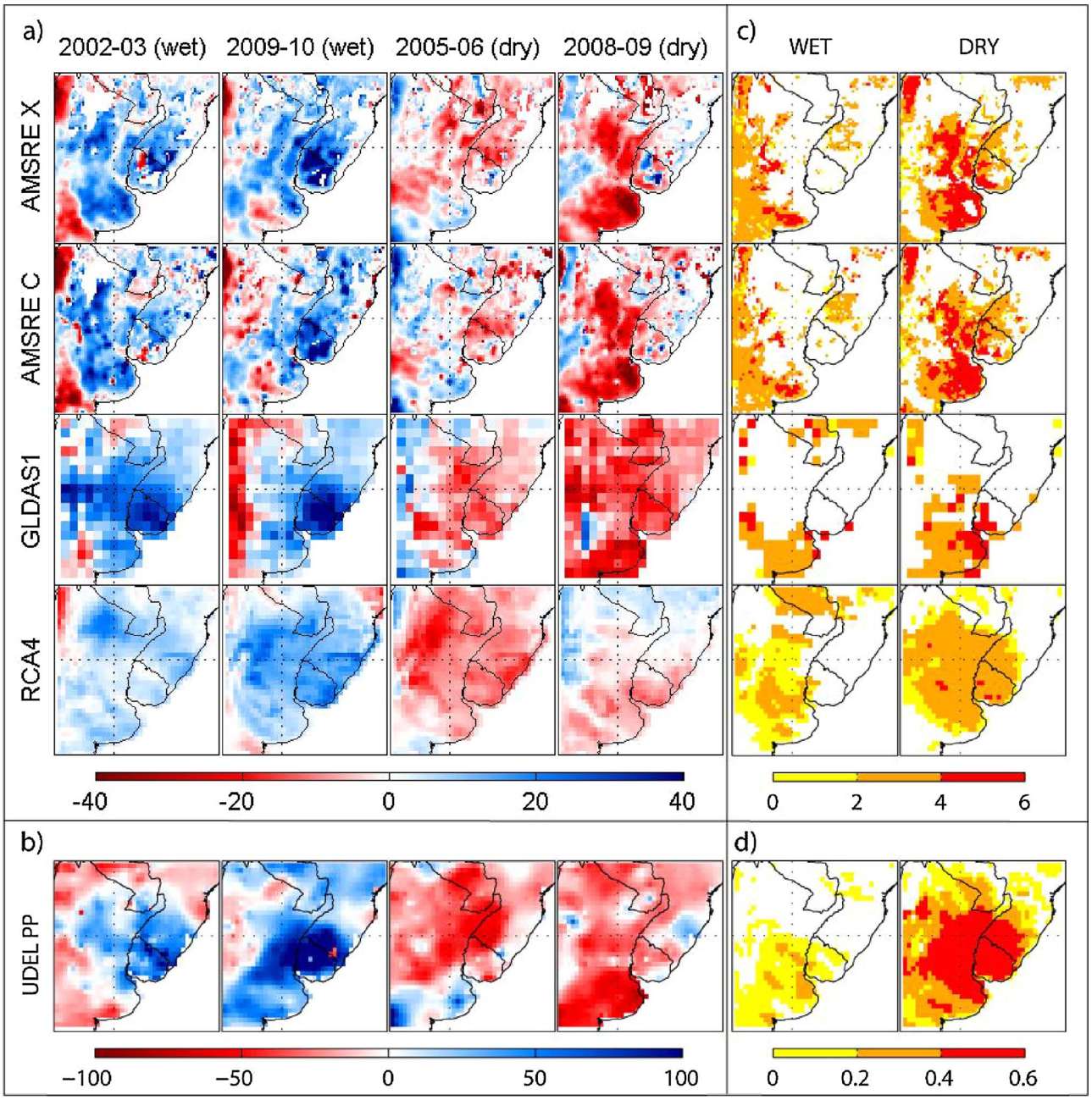

Fig. 5. Relative (%) mean seasonal anomalies of a) top SM from AMSRE-LPRM (X and C-bands), GLDAS-1 and RCA4 and b) UDEL precipitation (University of Delaware, Willmott and Matsuura, 2001) for wet (2002-03 and 2009-10) and dry (2005-06 and 2008-09) summers. c) L-A interaction index (I_{Temp}) for AMSRE-LPRM and MODIS LST, GLDAS-1 and RCA4 for these wet and dry summers(99% confidence interval, two tail t-Test) d) Coupling index for other dry and wet summers adapted from Ruscica et al. (2015).

and promising. In addition, based on the surface SM more rapidly variations compared to root zone SM, the time scale used within the L-A interaction metric is an important factor to be considered.

For this application (L-A interaction), the need of a consistent and long enough time series of SM satellite products has limited the use of existing L-band passive microwave systems. Nevertheless, the differences observed in intensity under dry conditions (satellite vs. models) and in the spatial extent when comparing dry vs. wet L-A from previous studies, deserves further analysis based on L-band satellite SM products which are less sensitive to vegetation optical depth combined with more complex LSMs including for example interactive carbon cycle and a higher vertical discretization of the soil.

This study is a meeting point and a first collaboration between remote sensing and climate modeling communities of Argentina, in a region with the highest agricultural and livestock production of the continent, but with an important lack of in-situ SM observations availability.

Acknowledgments

This work was partially funded by the Inter-American Institute for Global Change Research (IAI) CRN 3035, which is supported by the U.S. National Science Foundation under Grant GEO-1128040.

MODIS LST data product was retrieved from the online Data Pool, courtesy of the NASA Land Processes Distributed Active Archive Center (LP DAAC), USGS/Earth Resources Observation and Science (EROS), Center Sioux Falls, South Dakota, https://lpdaac.usgs.gov/data_access/data_pool.

AMSRE-LPRM data product was obtained by Vrije Universiteit Amsterdam and NASA GSFC and retrieved from Goddard Earth Sciences

Data and Information Service Center (GES-DISC).

The GLDAS-1 data used in this study were acquired as part of the mission of NASA's Earth Science Division and archived and distributed by theGoddardEarth Sciences (GES) Data and Information Services Center (DISC).

UDel_AirT_Precip data was provided by the NOAA/OAR/ESRL PSD, Boulder, Colorado, USA, from their Web site at http://www.esrl.noaa.gov/psd/.

RCA4 simulations were made with the high-performance computing clusters available at CIMA/UBA-CONICET, Argentina.

References

Abelen, S., Seitz, F., Abarca-del-Rio, R., Güntner, A., 2015. Droughts and floods in the La Plata basin in soil moisture data and GRACE. Remote Sens. 7 (6), 7324–7349.

Barret, B.W., Dwyer, E., Whelan, P., 2009. Soil moisture retrieval from active spaceborne microwave observations: an evaluation of current techniques. Remote Sens. 1, 210–242.

Boulanger, J.P., Schlindwein, S., Gentile, E., 2011. CLARIS LPB WP1: metamorphosis of the CLARIS LPB European project: from a mechanistic to a systemic approach. CLIVAR Exchanges 16–57, 7–10.

Dirmeyer, P.A., 2011. The terrestrial segment of soil moisture–climate coupling. Geophys. Res. Lett. 38, L16702. http://dx.doi.org/10.1029/2011GL048268.

Dorigo, W.A., et al., 2011. The International Soil Moisture Network: a data hosting facility for global in situ soil moisture measurements. Hydrol. Earth Syst. Sci. 15, 1675–1698. http://dx.doi.org/10.5194/hess-15-1675-2011.

Du, E., Di Vittorio, A., Collins, W., 2016. Evaluation of hydrologic components of community land model 4 and bias identification. Int. J. Appl. Earth Obs. Geoinf. 48, 5–16. http://dx.doi.org/10.1016/j.jag.2015.03.013.

Ek, M.B., et al., 2003. Implementation of Noah land surface model advances in the National Centers for Environmental Prediction operational mesoscale Eta model. J. Geophys. Res. 108 (D22), 8851. http://dx.doi.org/10.1029/2002jd003296.

Entekhabi, D., Reichle, R.H., Koster, R.D., Crow, W.T., 2010. Performance metrics for soil moisture retrievals and application requirements. J. Hydrometeor 11, 832–840. http://dx.doi.org/10.1175/2010JHM1223.1.

Ferguson, C.R., Wood, E.F., Vinukollu, K., 2012. A global intercomparison of modeled and observed land–atmosphere coupling. J. Hydrometeor 13, 749–784. http://dx.doi.org/10.1175/JHM-D-11-0119.1.

Gallego-Elvira, B., Taylor, C.M., Harris, P.P., Ghent, D., Veal, K.L., Folwell, S.S., 2016. Global observational diagnosis of soil moisture control on the land surface energy balance. Geophys. Res. Lett. 43, 2623–2631. http://dx.doi.org/10.1002/2016GL068178.

Hirschi, M., Mueller, B., Dorigo, W., Seneviratne, S.I., 2014. Using remotely sensed soil moisture for land-atmosphere coupling diagnostics: the role of surface vs. root-zone soil moisture variability. Rem. Sensing. Environ. 154, 246–252. http://dx.doi.org/10.1016/j.rse.2014.08.030. (ISSN 0034-4257).

Jackson, T.J., 1993. Measuring surface soil moisture using passive microwave remote sensing. Hydrol. Process. 7 (2), 139–152 (John Wiley & Sons, Ltd.).

Jung, M., et al., 2010. Recent decline in the global land evapotranspiration trend due to limited moisture supply. Nature 467 (7318), 951–954. http://dx.doi.org/10.1038/nature09396.

Koster, R.D., 2004. Regions of strong coupling between soil moisture and precipitation. Science 305, 1138–1140. http://dx.doi.org/10.1126/science.

Lehner, B., Verdin, K., Jarvis, A., 2006. HydroSHEDS, Technical Documentation, Version 1.0. (Available online at: http://hydrosheds.cr.usgs.gov/webappcontent/HydroSHEDS_TechDoc_v10.pdf).

Martens, B., Miralles, D., Lievens, H., Fernández-Prieto, D., Verhoest, N.E.C., 2016. Improving terrestrial evaporation estimates over continental Australia through assimilation of SMOS soil moisture. Int. J. Appl. Earth Obs. Geoinf. 48, 146–162.

Global scale estimation of land surface heat fluxes from space: current status and future trends. In: Petropoulos, G.P. (Ed.), Remote Sensing of Land Surface Turbulent Fluxes and Soil Surface Moisture Content: State of the Art. Taylor & Francis.

Meesters, A.C.G.A., DeJeu, R.A.M., Owe, M., 2005. Analytical derivation of the vegetation optical depth from the microwave polarization difference index. IEEE Geosci. Remote Sens. Lett. 2 (2), 121–123.

Mladenova, I.E., et al., 2014. Remote monitoring of soil moisture using passive microwave-based techniques.Theoretical basis and overview of selected algorithms for AMSR-E. Remote Sens. Environ. 144, 197–213. http://dx.doi.org/10.1016/j.rse.2014.01.013. (ISSN 0034-4257).

Mo, K., Berbery, E.H., 2011. Drought and persistent wet spells over south america based on observations and the U.S CLIVAR drought experiments. J. Clim. 24, 1801–1820.

Mo, T., Choudhury, B.J., Schmugge, T.J., Jackson, T.J., 1982. A model for microwave emission from vegetation-covered fields. J. Geophys. Res 87 (December 20), 11,229–11,237 (C13).

Mueller, B., Seneviratne, S.I., 2012. Hot days induced by precipitation deficits at the global scale. Proc. Natl. Acad. Sci. U. S. A. 109 (31), 12,398–12,403. http://dx.doi.org/10.1073/pnas.1204330109.

Njoku, E.G., Jackson, T.J., Lakshmi, V., Chan, T.K., Nghiem, S.V., 2003. Soil moisture retrieval from AMSR-E. IEEE Trans. Geosci. Remote Sens. 41, 215–229.

Norouzi, H., Temimi, M., Rossow, W.B., Pearl, C., Azarderakhsh, M., Khanbilvardi, R., 2011. The sensitivity of land emissivity estimates from AMSR-E at C and X bands to surface properties. Hydrol. Earth Syst. Sci. 15, 3577–3589. http://dx.doi.org/10.5194/hess-15-3577-2011.

Notarnicola, C., Angiulli, M., Posa, F., 2006. Use of radar and optical remotely sensed data for soil moisture retrieval on vegetated areas. IEEE Trans. Geosci. Remote Sens. 44, 925–935.

Notaro, M., 2008. Statistical identification of global hot spots in soil moisture feedbacks among IPCC AR4 models. J. Geophys. Res. 113http://dx.doi.org/10.1029/2007jd009199. (D09101).

Olson, D.M., 2001. Terrestrial ecoregions of the world: a new map of life on Earth. Bioscience 51 (11), 933–938.

Reichle, R.H., Koster, R.D., De Lannoy, G.J.M., Forman, B.A., Liu, Q., Mahanama, S.P.P., Touré, A., 2011. Assessment andenhancement of MERRA land surface hydrology estimates. J. Clim. 24, 6322–6338. http://dx.doi.org/10.1175/JCLID-10-05033.1.

Rodell, M., et al., 2004. The global land data assimilation system. Bull. Am. Meteorol. Soc. 85, 381–394. http://dx.doi.org/10.1175/BAMS-85-3-381.

Ruscica, R.C., 2015. Procesos de acople e interacción superficie-atmósfera en el sudeste de Sudamérica. PhD Thesis. Faculty of Exact and Natural Sciences. University of Buenos Aires.

Ruscica, R.C., Sörensson, A.A., Menéndez, C.G., 2014. Hydrological links in Southeastern South America: soil moisture memory and coupling within a hot spot. Int. J. Climatol. 34, 3641–3653. http://dx.doi.org/10.1002/joc.3930.

Ruscica, R.C., Sörensson, A.A., Menéndez, C.G., 2015. Pathways between soil moisture andprecipitation in southeastern South America. Atm. Sci. Lett. http://dx.doi.org/10.1002/asl2.552.

Ruscica, R.C., Menéndez, C.G., Sörensson, A.A., 2016. Land surface–atmosphere interaction in future South American climate using a multi-model ensemble. Atm. Sci Lett. 17, 141–147. http://dx.doi.org/10.1002/asl.63.

Sörensson, A.A., Menéndez, C.G., 2011. Summer soil-precipitation coupling in south america. Tellus Ser A: Dyn. Meteorol. Oceanogr. 63, 56–68. http://dx.doi.org/10.1111/j.1600-0870.2010.00468.x.

Sörensson, A.A., 2010. Análisis de retroalimentaciones suelo-atmósfera en América del Sur empleando un nuevo modelo climático regional. PhD Thesis. Faculty of Exact and Natural Sciences. University of Buenos Aires.

Sakai, T., et al., 2016. Varying applicability of four different satellite-derived soil moisture products to global gridded crop model evaluation. Int. J. Appl. Earth Obs. Geoinf. 48, 51–60. http://dx.doi.org/10.1016/j.jag.2015.09.011.

Samuelsson, P., Jones, Colin, Willéna, Ulrika, Ullerstig, Anders, 2011. The rossby centre regional climate model RCA3: model description and performance. Tellus Ser. A-Dyn. Meteorol. Oceanogr. 63A (1), 4–23. http://dx.doi.org/10.1111/j.1600-0870.2010.00478.x.

Sato, H., Akihiko, I., Akinori, I., Takashi, I., Etsushi, K., 2015. Current status and future of land surface models. Soil Sci. Plant Nutr. 61 (1), 34–47. http://dx.doi.org/10.1080/00380768.2014.917593.

Seneviratne, S., et al., 2010. Investigating soil moisture-climate interactions in a changing climate: a review. Earth Sci. Rev. 99 (3–4), 125–161. http://dx.doi.org/10.1016/j.earscirev.2010.02.004. (ISSN 0012-8252).

Spennemann, P.C., Saulo, A.C., 2015. An estimation of the land-atmosphere coupling strength in South America using the Global Land Data assimilation system. Int. J. Climatol. 35, 4151–4166. http://dx.doi.org/10.1002/joc.4274.

Stensrud, 2007. Parameterization Schemes: Keys To Understanding Numerical Weather Prediction Models. Cambridge University Press.

Wan, Z., Dozier, J., 1996. A generalized split-window algorithm for retrieving landsurface temperature from space. IEEE Trans. Geosci. Remote Sens. 34 (4), 892–905.

Wan, Z., 1999. MODIS land surface temperature Algorithm Theoretical Basis Document (LST ATBD), version 3.3. (Available online at: https://modis.gsfc.nasa.gov/data/atbd/atbd_mod11.pdf).

Wan, Z., 2006. Collection 5. MODIS Land surface temperature products user's guide. (Available online at: http://icess.eri.ucsb.edu/modis/LstUsrGuide/MODIS_LST_products_Users_guide_C5.pdf).

Wang, G., Kim, Y., Wang, D., 2007. Quantifying the strength of soilmoisture-precipitation coupling and its sensitivity to changes in surfacewater budget. J. Hydrometeorol. 8, 551–570. http://dx.doi.org/10.1175/JHM573.1.

Willmott, C.J., Matsuura, K., 2001. Terrestrial Air Temperature and Precipitation: Monthly and Annual Time Series (1950–1999). http://climate.geog.udel.edu/~climate/html_pages/README.ghcn_ts2.html.

Zeng, X., Barlage, M., Castro, C., Fling, K., 2010. Comparison of land–precipitation coupling strength using observations and models. J. Hydrometeor 11, 979–994.

Zhou, J., Lau, K.M., 2001. Principal modes of interannual and decadal variability of summer rainfall over South America. Int. J. Climatol. 21 (13), 1623–1644.

Zhou, J., Zhang, X., Zhanand, W., Zhang, H., 2014. Land surface temperature retrieval from MODIS data by integrating regression models and the genetic algorithm in an arid region. Remote Sens. 2014 (6), 5344–5367. http://dx.doi.org/10.3390/rs6065344.